ADVANCED FUNCTIONAL MATERIALS
www.afm-journal.de

A Bio-Conjugated Fullerene as a Subcellular-Targeted and Multifaceted Phototheranostic Agent

Matteo Di Giosia, Alice Soldà, Markus Seeger, Andrea Cantelli, Fabio Arnesano, Maria I. Nardella, Vincenzo Mangini, Francesco Valle, Marco Montalti, Francesco Zerbetto, Stefania Rapino, Matteo Calvaresi, and Vasilis Ntziachristos**

Fullerenes are candidates for theranostic applications because of their high photodynamic activity and intrinsic multimodal imaging contrast. However, fullerenes suffer from low solubility in aqueous media, poor biocompatibility, cell toxicity, and a tendency to aggregate. C_{70}@lysozyme is introduced herein as a novel bioconjugate that is harmless to a cellular environment, yet is also photoactive and has excellent optical and optoacoustic contrast for tracking cellular uptake and intracellular localization. The formation, water-solubility, photoactivity, and unperturbed structure of C_{70}@lysozyme are confirmed using UV-visible and 2D ^{1}H, ^{15}N NMR spectroscopy. The excellent imaging contrast of C_{70}@lysozyme in optoacoustic and third harmonic generation microscopy is exploited to monitor its uptake in HeLa cells and lysosomal trafficking. Last, the photoactivity of C_{70}@lysozyme and its ability to initiate cell death by means of singlet oxygen ($^{1}O_2$) production upon exposure to low levels of white light irradiation is demonstrated. This study introduces C_{70}@lysozyme and other fullerene-protein conjugates as potential candidates for theranostic applications.

1. Introduction

Phototheranostics,[1,2] based on the integration of light-induced imaging and therapeutic modalities, has attracted considerable attention in recent years as a highly promising approach to non-invasive cancer treatment via photodynamic therapy (PDT).[3,4] PDT is a clinically approved phototherapeutic procedure, which uses light and specific molecules with photosensitizing properties[5] to induce a selective cytotoxic activity towards malignant cells. However, the design of phototheranostic agents (PTAs) is hindered by several conflicting needs and unmet requirements. The desired stimuli-responsive agents, typically referred to as photosensitizers (PS), should on the one hand generate high concentrations of reactive oxygen species (ROS) upon irradiation with light to initiate cell death in a targeted manner, while on the other hand display negligible toxicity in dark conditions. They must also have high solubility in biological systems and the ability to target and accumulate in specific cells, as expected from 3rd generation PSs.[6] Last, these agents should provide imaging contrast to allow monitoring of their bio-distribution or treatment efficacy and possibly reveal mechanisms of action during research and development.[7]

A PTA may either be a single-entity species or a nanomaterial conjugated and/or loaded with different imaging and therapeutic agents.[3,4] The single-entity approach reduces the synthetic burden and thus the variability of phototheranostic performance. PTAs can be classified into inorganic or organic materials.[8] Among organic materials, porphyrinoid derivatives and precursors are the most commonly used PTAs, especially for clinical applications.[9] These molecules can produce significant amounts of ROS upon excitation because of their intense absorption in the visible range. Their main limitations are photobleaching and aggregation, which lead to a steady decrease in their efficacy as both ROS producers and contrast agents. In contrast, inorganic PTAs typically display higher photostability than their organic counterparts. Widely used gold nanostructures afford versatile probes for both luminescent[10] and optoacoustic (OA, also termed photoacoustic)[11,12] imaging applications; nevertheless, they do not adequately perform as PS. Gold, as well as other noble metal-based nanoparticles, are often expensive, non-degradable, and require toxic surfactants for their syntheses,

Dr. M. Di Giosia, Dr. A. Cantelli, Prof. M. Montalti, Prof. F. Zerbetto, Prof. S. Rapino, Prof. M. Calvaresi
Dipartimento di Chimica "Giacomo Ciamician"
Alma Mater Studiorum—Università di Bologna
via Francesco Selmi 2, Bologna 40126, Italy
E-mail: matteo.calvaresi3@unibo.it

Dr. A. Soldà, Dr. M. Seeger, Prof. V. Ntziachristos
Chair of Biological Imaging
Center for Translational Cancer Research (TranslaTUM)
Technical University of Munich
81675 Munich, Germany
E-mail: v.ntziachristos@tum.de

Dr. A. Soldà, Dr. M. Seeger, Prof. V. Ntziachristos
Institute of Biological and Medical Imaging (IBMI)
Helmholtz Zentrum München
85764 Munich, Germany

Prof. F. Arnesano, Dr. M. I. Nardella, Dr. V. Mangini
Dipartimento di Chimica
Università di Bari "A. Moro"
via E. Orabona 4, Bari 70125, Italy

Dr. F. Valle
Istituto per lo Studio dei Materiali Nanostrutturati (CNR-ISMN)
Consiglio Nazionale delle Ricerche
via P. Gobetti 101, Bologna 40129, Italy

The ORCID identification number(s) for the author(s) of this article can be found under https://doi.org/10.1002/adfm.202101527.

DOI: 10.1002/adfm.202101527

which must be avoided for clinical translation.[8,13] Quantum dots are also suitable probes for high-contrast in vitro and in vivo imaging thanks to their strong fluorescence emission upon visible light or NIR light excitation.[14] However, their quantum yield of ROS production is low compared to standard PSs.[6,15] Metal-oxide semiconducting nanomaterials (i.e., TiO_2 and ZnO) have been widely applied as UV light-triggered PSs because of their large bandgap, good chemical stability, low cost, and nontoxicity advantages.[16–18] However, despite their outstanding performance as PSs, their application is limited by low solubility in physiological environments, high cytotoxicity, and the poor depth penetration of the UV light required for their excitation.

Graphitic carbon-based molecules and nanomaterials have shown promise for imaging and therapeutic applications.[19] Fullerenes in particular have unique electronic and physical properties that make them attractive candidates for theranostics.[20–26] Fullerenes are characterized by high photostability,[27–30] broad UV-visible light absorption, and efficient light stimulated production of ROS by both type I and II mechanisms[27–30] or heat.[31–33] They are excellent electron acceptors, which also enable oxygen-independent photo-killing.[34] Beyond their PS properties, fullerenes also produce ROS upon ultrasound wave irradiation.[35,36]

Besides their PDT functionalities, fullerenes feature excellent contrast for both OA and third-harmonic generation (THG) imaging techniques.[31,33,37] OA imaging relies on the detection of acoustic waves that are generated upon non-radiative deexcitation after the absorption of light energy. Fullerenes are ideal OA imaging agents because they exhibit broad absorption across the UV-visible spectral range with negligible quantum yields. THG imaging is sensitive to local differences in third-order nonlinear properties and changes in refractive index. Fullerenes afford excellent THG contrast by greatly altering the local refractive index[38–40] due to the delocalization of their π-electron conjugated systems and their hollow structures.

However, using fullerenes in theranostics or other biological applications has in many cases been impeded by their hydrophobicity, which makes them prone to aggregation in aqueous media, reduces their bio-compatibility,[41] leads to quenching of the triplet excited state,[42–44] and decreases the active surface area available for ROS production. One means of effectively dispersing fullerenes in aqueous media, while preventing modification of their molecular structures, is through the use of supramolecular solubilizing agents.[45–47] Proteins and peptides can be used as biocompatible hosts for fullerenes, allowing the dispersion of fullerenes as single molecules in physiological environments to prevent aggregation phenomena.[48–53] In particular, lysozyme binds and disperses C_{60} in water, and the resulting C_{60}@lysozyme complex is still photoactive, generating significant quantities of ROS upon visible light irradiation, while remaining biocompatible in dark conditions.[48] It was shown that irradiation of C_{60}@lysozyme with visible light significantly reduced the viability of HeLa cells in vitro, making it a candidate for PDT.[54] However, the localization, uptake mechanism, and cell targeting properties of this complex have not been investigated.

We hypothesized that the high intrinsic OA and THG contrasts of fullerenes would enable tracking of the uptake and localization of fullerene-protein complexes in cancer cells, thus enabling studies into their theranostic applications. To test this hypothesis, we chose to synthesize and investigate a lysozyme complex comprising C_{70}, as this fullerene has a broader absorption profile than C_{60} (required for OA imaging, Section S1, Supporting Information) and high photodynamic activity.[55–58]

Herein, we present this new C_{70}@lysozyme complex, along with a thorough study of its biocompatibility, cellular uptake, and photodynamic activity. Using 2D ^{1}H, ^{15}N NMR we evaluate whether C_{70}@lysozyme maintains the structure of the native protein, and thus its ability to cross the cell membrane and to accumulate in subcellular organelles.[59,60] Such accumulation is necessary to enhance both PDT efficacy and imaging contrast. We exploit the multimodal imaging contrast of C_{70} to monitor the uptake of C_{70}@lysozyme in cancer cells using co-registered and simultaneous OA and THG microscopy. In particular, we employ OA imaging to monitor the trafficking of the C_{70}@lysozyme into living cells. Furthermore, we employ fluorescent labels and two-photon excitation fluorescence (2PEF) microscopy, in parallel with OA and THG microscopy, to validate the localization of C_{70}@lysozyme at the subcellular level, and in particular its accumulation within the lysosomes. Finally, we confirm the photoactivity of C_{70}@lysozyme and its ability to initiate cell death upon irradiation with white light by means of intracellular singlet oxygen ($^{1}O_2$) production. This study not only introduces C_{70}@lysozyme as a novel and selective PTA, but also showcases the powerful multimodal contrast of biocompatible fullerene-protein bioconjugates.

2. Results and Discussion

We prepared monodispersed C_{70} by host-guest interaction with lysozyme in the form of a C_{70}@lysozyme bioconjugate, constituting a non-covalent supramolecular complex. The UV-visible absorption spectrum of the C_{70}@lysozyme in water (**Figure 1**A) revealed features that belong to both components of the bioconjugate, demonstrating the attainment of water solubility of C_{70}. Comparing the photophysical data reported by Ke et al. for dispersion of C_{70} in water (Section S2, Figure S2.1, Supporting Information),[61] the herein found absorbance is consistent with a concentration of solubilized C_{70} similar to that of lysozyme, supporting the formation of a stable stoichiometric 1:1 complex of C_{70}@lysozyme.[49] In addition, the colloid stability of C_{70}@lysozyme was tested by UV-visible kinetic analysis (Section S2, Figure S2.2, Supporting Information). The results demonstrate that the complex is stable for at least three hours in static conditions, corresponding to the incubation time for the in vitro PDT assay.

Chemical shift perturbation analysis of the 2D ^{1}H, ^{15}N NMR spectra confirmed that, upon C_{70} binding, lysozyme retains its 3D folding (Sections S3 and S4, Supporting Information), similar to the observations for the binding of C_{60}.[49,58] Compared to C_{60}@lysozyme,[49] the chemical shift perturbations induced upon C_{70} binding involve more amino acid residues, indicating that the bulkier C_{70} either induces some conformational changes outside the fullerene binding

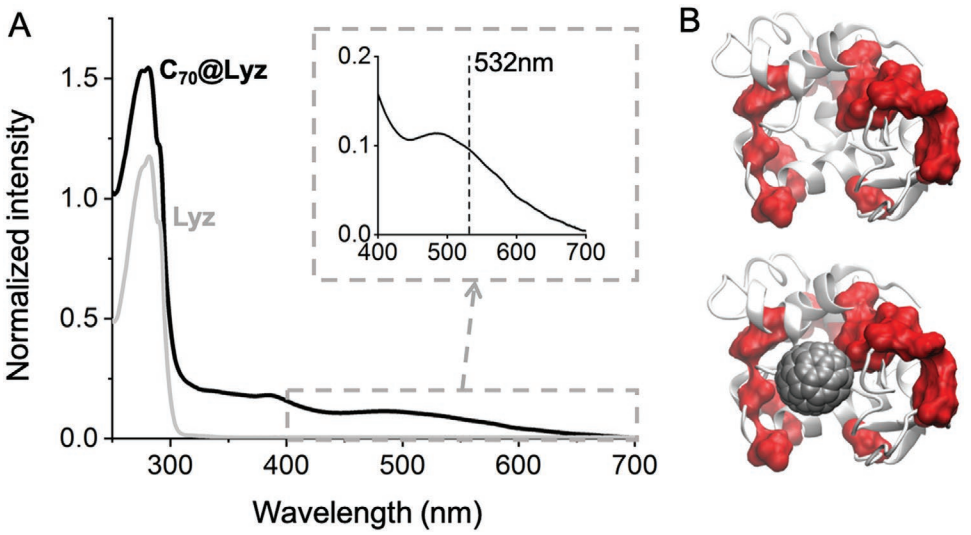

Figure 1. A) UV-visible spectra of lysozyme (grey line) and the C_{70}@lysozyme (black line). The inset shows the UV-visible spectrum of C_{70}@lysozyme in the 400–700 nm range with the dotted line indicating the emission wavelength of the solid-state laser (532 nm) used for recording the OA images (vide infra). B) 3D representations of lysozyme (top) and C_{70}@lysozyme (bottom). The residues that undergo the largest changes in NMR chemical shifts upon C_{70} binding are highlighted in red (Section S3, Figure S3, Supporting Information).

site, or that protein-protein interactions occur that shield the exposed surface area of the fullerene from the polar environment.

Atomic force microscopy (AFM) of C_{70}@lysozyme (Section S5, Figure S5, Supporting Information) showed that, although a monomolecular dispersion of the bioconjugates over the mica surface is evident, oligomeric structures are also present. This is in agreement with previous characterizations of lysozyme as a protein with a strong tendency to self-associate in aqueous solution, forming dimeric and trimeric structures,[62] in addition to effects induced by dehydration. However, AFM investigations performed on multiple random areas on the mica surface, both at high and low magnification, did not show any presence of nanoaggregates. The combination of UV-visible, 2D-NMR, and AFM analysis (Sections S1–S4, Supporting Information) demonstrates that the fullerenes are dispersed by lysozyme in aqueous media in a stoichiometric manner, as single molecules, rather than as NPs.

Upon visible light illumination, C_{70} sensitizes the production of singlet oxygen. The production of singlet oxygen can be measured either directly, by its radiative decay at 1270 nm (phosphorescence), or indirectly using a singlet oxygen fluorescent probe (e.g., SOSG).[63,64] In order to evaluate quantitatively the photosensitizing ability of C_{70}@lysozyme, the production of singlet oxygen ($^1O_2$) in water upon visible light irradiation was herein measured using the phosphorescence of $^1O_2$ at 1270 nm. The quantum yield of $^1O_2$ generation by C_{70}@lysozyme was determined by comparing it with that obtained by a standard PS (Rose Bengal (RB), Φ_Δ = 0.76 in D_2O solution).[65] The phosphorescence spectra of isoabsorbing solutions of C_{70}@lysozyme and RB, at the excitation wavelength (λ_{exc} = 514 nm), are shown in Figure S6, Section S6, Supporting Information. C_{70}@lysozyme was found to have a Φ_Δ of 0.60. More importantly, when the experiment was repeated in water, the RB did not produce a detectable quantity of $^1O_2$, while C_{70}@lysozyme produced significant amounts (Φ_Δ of 0.31, compared to Φ_Δ of RB in D_2O). This effect might be due to the confinement of C_{70} in the lysozyme binding pocket, with the hydrophobic protein enabling generation of $^1O_2$ by shielding the sensitizing C_{70} chromophores from quenching by water molecules.[66] The ability to produce ROS in water is crucial for the effective application of PDT in real physiological environments. In addition, C_{70}@lysozyme generates $^1O_2$ with excitation throughout the visible range (Figure S6, Supporting Information), which enlarges its potential for practical applications.

Due to the insolubility of C_{70} in water and water-miscible solvents, standard methodologies for determining binding energy, such as ITC or fluorescence titration analysis,[67] cannot be performed for C_{70} and lysozyme. Nevertheless, we determined the binding affinity between the two interacting systems using a computational protocol, which was recently validated to calculate the binding energy between proteins and fullerenes (Section S7, Supporting Information). The binding affinity ($\Delta G_{binding}$) between C_{70} and lysozyme is –19.9 kcal mol^{-1}. In addition, we provide an accurate analysis of the thermodynamic of binding between C_{70} and lysozyme: the total binding energy was decomposed into their binding components and the contribution to the binding of each amino acid was calculated (Section S7, Supporting Information).

We assessed the cytotoxicity and phototoxicity of C_{70}@lysozyme at different concentrations upon photoexcitation with visible light (white-light LED) by testing its ability to inhibit growth and induce death in HeLa cells. **Figure 2** shows that a small reduction in cell viability or a potential inhibition of cell growth was observed in darkness only at a high concentration of C_{70}@lysozyme (>5 μM). In contrast, irradiation of HeLa cells with visible light at ultralow light power (irradiance 2 mW cm^{-2}) for 10 min in the presence of C_{70}@lysozyme caused an increase in the cell mortality in a dose-dependent

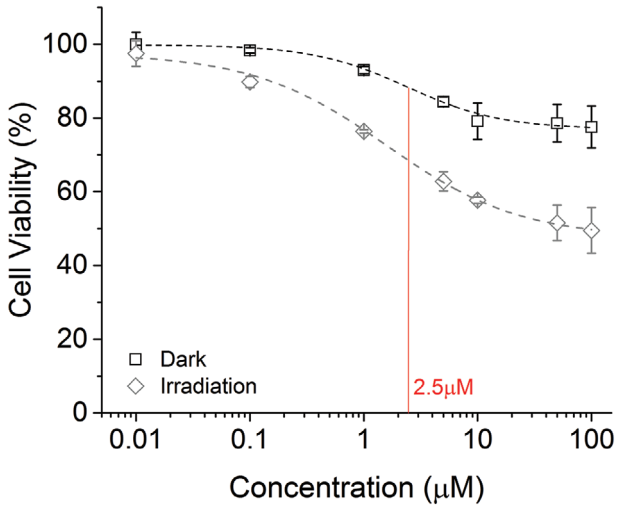

Figure 2. Effect of 3h incubation with C_{70}@lysozyme on HeLa cell viability in both dark conditions (black boxes) and upon 10 min of visible light irradiation (grey diamonds). Each sample was measured 24 h after treatment with C_{70}@lysozyme. Each box and bar represent the mean value ± standard deviation (SD) of three replicates. The dotted lines represent the Hill fitting of the dose response assay. The red line indicates a concentration of 2.5 μM, which was employed for the subsequent subcellular studies performed in living cells.

manner. No reduction in viability was observed upon the irradiation of untreated cells within the same time period (Section S8, Supporting Information).

We next tested the optical and OA characteristics of C_{70}@lysozyme to investigate its potential as a contrast agent for phototheranostics. Using a custom-built hybrid microscopy system,[68–73] which combines optical-resolution OA, THG, and 2PEF microscopy, we clearly demonstrated that C_{70} generates significant THG response (Figure S9A, Supporting Information) as well as intense OA signal (Figure S9B, Section S9, Supporting Information) when dispersed on a microscope slide.

Having confirmed the strong OA and THG contrast generated by C_{70}@lysozyme, we investigated its uptake and subcellular distribution in living cells. This was done by performing time-course studies on HeLa cells in vitro under physiological conditions for real cell live imaging (i.e., 37 °C, 5% CO_2, and 80% humidity) using a stage top incubator. We imaged cultured cells in time steps of 15 min for up to 4 h of incubation with OA only, as parallel THG measurements would increase the potential of inducing cell death via PDT or photothermal ablation over long time exposure.

Figure 3 shows that no significant uptake is observed during the first hour, while sub-resolution point-like signals are detected for OA after approximately 1.5 h. The application of particle-analysis methods showed that the uptake-trajectories peaked in terms of the number of signals and total area coverage at 3 h (Figure 3D). Furthermore, the mean value (≈ 200 a.u.) of the signals remained constant, which indicates high regularity of C_{70}@lysozyme trafficking driven by the intrinsic cellular behavior. Both the constant amplitude and the subcellular spatial extent of the signal suggest lysosomal accumulation of C_{70}@lysozyme and the conservation of the "biological identity" of the carrier protein.[59,60] Brightfield images were taken before and after the experiment to confirm the healthy state of the cells during the measurements (Section S10, Supporting Information).

Finally, we tested the lysosomal localization of C_{70}@lysozyme by fluorescently labeling lysosomes (LysoTracker) for 2PEF readings (excitation wavelength 521.5 nm), which were performed with the identical microscope used for OA and THG imaging. We were able to co-localize the majority of the C_{70}@lysozyme into the lysosomes after 3 h post washout (**Figure 4**). Both the THG and OA signals were resolved, which revealed a co-localized pattern that offers the possibility to detect fullerene distribution without immunolabeling[74] and without attaching imaging tags to its cage,[75] which could perturb the properties of fullerene and its real distribution. The high spatial correlation between OA and THG, calculated using the Pearson Correlation Coefficient (PCC), confirms its dual-modal contrast in subcellular compartments. The non-vanishing, but relatively low, PCC to 2PEF readings suggest that while there is abundant lysosomal localization of C_{70}@lysozyme, there are also some lysosomes that are labeled but agent-empty, as well as some unspecific fluorescence signal evoked from the cell

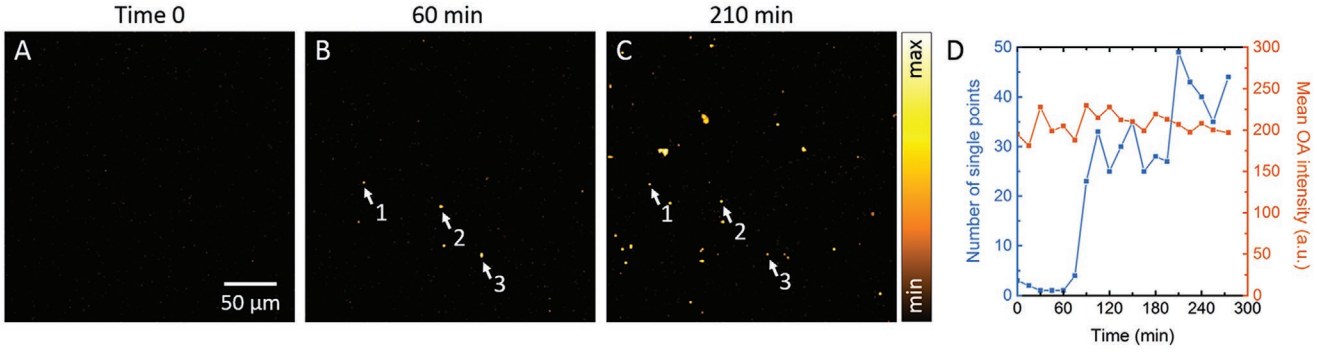

Figure 3. Time-course of the OA signal of C_{70}@lysozyme suggesting lysosomal trafficking in HeLa cells upon 4 h incubation. OA images are taken at times A) 0, B) 60, and C) 210 min. D) Point-source analysis demonstrates an increase from 0 to around 40 point-like signals (blue line), while the mean OA intensity (orange line) of the recorded point-like signals remains stable. Point-source analysis gives information about the number of the particles in focus during the measurement, while the stable mean values demonstrate the ability of the C_{70}@lysozyme to be internalized by the cells and then ejected without affecting the cells themselves.

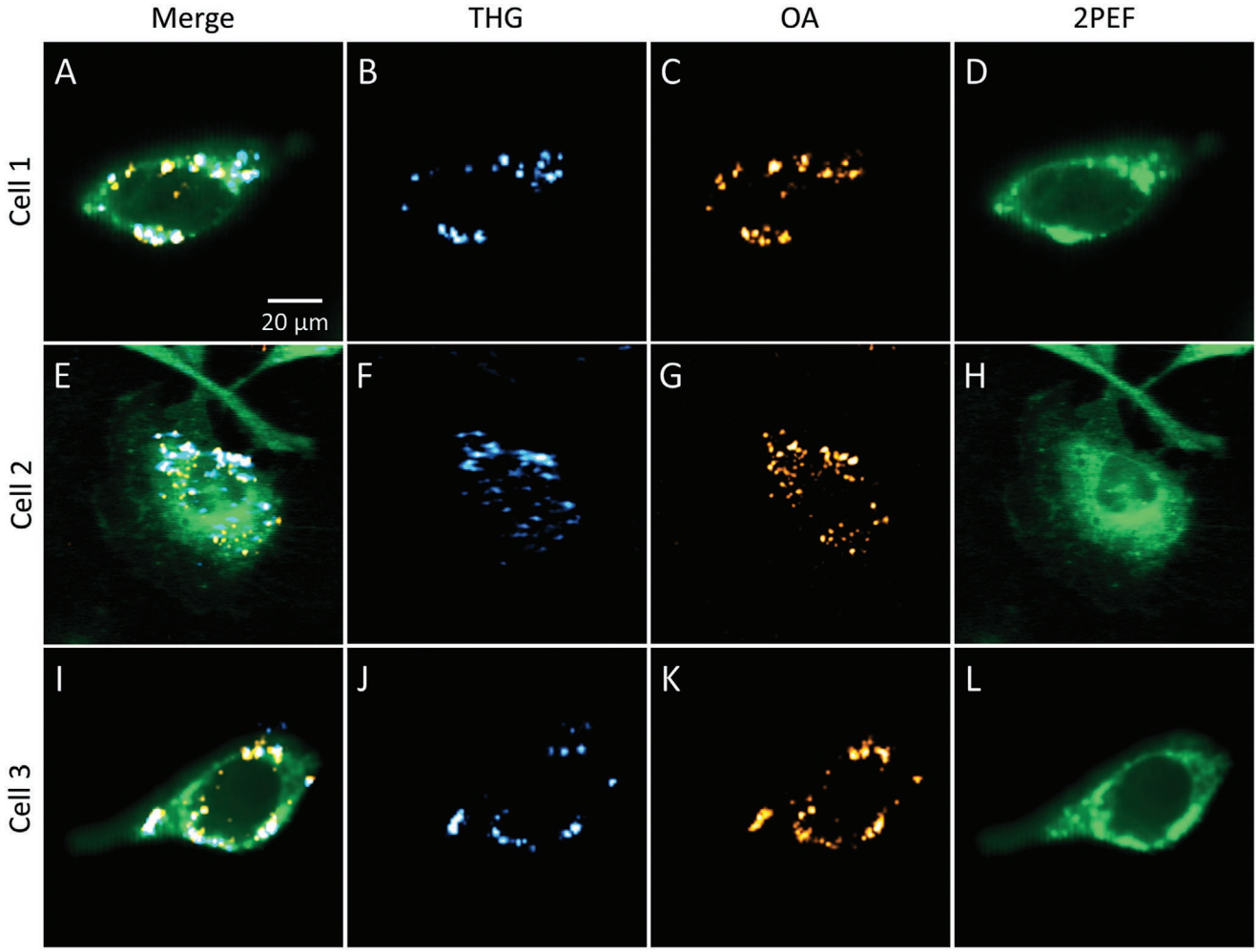

Figure 4. Co-localization of C_{70}@lysozyme into lysosomes in HeLa cells after 3 h incubation. A) Merged presentations of THG and OA signals arising from C_{70}@lysozyme, along with 2PEF signals arising from fluorescently labeled lysosomes (LysoTracker Deep Red) for a single isolated HeLa cell. Separate depictions of the (B) THG, (C) OA, and (D) 2PEF modalities. E–L) Analogous depictions for two other single HeLa cells. THG and OA modalities reveal a co-localized patterns with a PCC of 0.597 ± 0.036. THG and 2PEF modalities reveal a co-localized pattern with a PCC of 0.393 ± 0.056. OA and 2PEF modalities reveal a co-localized pattern with a PCC of 0.397 ± 0.028.

body. Hence, it can be assumed that all C_{70}@lysozyme is trafficked to lysosomes and all lysosomes are labeled, but not all lysosomes contain C_{70}@lysozyme. Analogous imaging experiments of HeLa cells with C_{70}@BSA showed no significant signal patterns in the THG and OA inside the cells, which suggests that C_{70}@BSA undergoes neither endocytic uptake nor trafficking to the lysosomes (Section S11, Supporting Information). The local accumulation of C_{70}@lysozyme inside cells is a significant advantage over C_{70}@BSA, since such an accumulation enhances both OA and THG imaging and C_{70}'s ability to generate ROS intracellularly.

Whereas THG and OA signals of C_{70}@lysozyme are only detectable within an intracellular compartment upon high local accumulation and sufficient size (>300 nm) due to sensitivity limitations of these modalities, the 2PEF signals can also arise from unbound fluorescent labels. Furthermore, whereas LysoTracker Deep Red is expected to label all lysosomes, we do not expect all lysosomes to contain sufficient C_{70}@lysozyme for THG and OA detection.

Finally, in order to test the photoactivity of bioconjugated C_{70}@lysozyme, we monitored the fluorescence of singlet oxygen sensor green (SOSG), whose fluorescence intensity increases in the presence of singlet oxygen (**Figure 5**). The measurement was performed at 20 min intervals (Section S12, Supporting Information), with either darkness or white light illumination between measurements. We used a high-power LED Module to excite the PS accumulated inside the cells, with a white light temperature of 850 lm.

The intensity of the fluorescence of SOSG increases by a factor of >4.2 when incubated together with C_{70}@lysozyme and white light illumination, which suggests significant production of singlet oxygen. Cells incubated only with the SOSG and illuminated with white light showed an increase of ≈2.7 due to the photoactivity of the sensor itself. When not illuminated with white light, SOSG-incubated cells with and without C_{70}@lysozyme increased their fluorescence by a factor of ≈1.5, due to the photoactivity induced by the laser used to excite the fluorescence of the SOSG sensor.

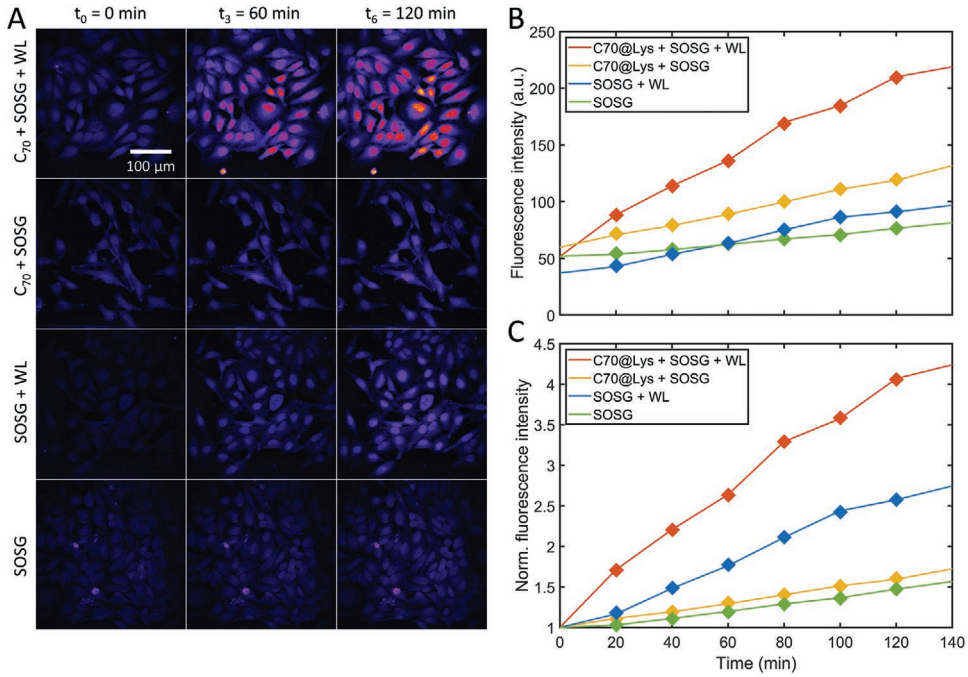

Figure 5. Photoactivity of C_{70}@lysozyme in HeLa cells. A) Photoactivity monitored with singlet-oxygen sensor green (SOSG), which increases its fluorescence in the presence of singlet oxygen. The measurement was obtained using 2PEF microscopy and was performed in 20 min steps with either darkness or white light illumination between measurements. A high-power LED Module (850 lm) was used to excite the PS accumulated inside the cells. Trajectories of (B) unnormalized and (C) normalized SOSG fluorescence intensity indicate an increase of >4.2 when incubated with C_{70}@lysozyme.

3. Conclusion

It is challenging to meet the many competing requirements for the development of a PTA, such as low toxicity, good contrast, targeted accumulation, and high ROS production capability. Herein, we demonstrate that C_{70}@lysozyme efficiently combines the optical and OA contrast and photosensitizing ability of C_{70} with the high solubility and monodispersity of lysozyme, overcoming previous limitations of using fullerenes in nanomedicine. Taking advantage of the high OA and THG contrast, we showed that C_{70}@lysozyme accumulates in lysosomes in cancer cells, which increases both imaging contrast and targeted cell-killing ability upon irradiation with visible light.

This work fully elaborates the capabilities of fullerene@protein complexes as image-guided PDT agents. As such complexes are highly adaptable, future work could aim at their functionalization both with tumor-targeting tags to improve the cancer cell selectivity and promote the cellular uptake of the photosensitizing agent,[76] and with light-harvesting molecular antennae[45,77–79] to improve both therapeutic efficiency and treatment depth in PDT.

In the future, we foresee C_{70}@lysozyme being employed as a PTA in vivo to enable both intracellular generation of singlet oxygen for targeted PDT and monitoring with mesoscopic or macroscopic imaging technology.

Supporting Information

Supporting Information is available from the Wiley Online Library or from the author.

Acknowledgements

M.D.G., A.S., and M.S. contributed equally to this work. The authors thank Robert J. Wilson for assisting with the editing of this manuscript. The authors thank Francesca Gasparin for assisting in the cell study during the revision process. The research leading to these results has received funding from AIRC under MFAG 2019–ID. 22894 project–P.I. M.C. This work was also supported by the Italian Ministry of Education, University and Research (MIUR), SIR Programme no. RBSI149ZN9–BIOTAXI funded to M.C. M.D.G. was supported by a FIRC-AIRC fellowship for Italy (id. 22318). The development of the herein utilized hybrid microscope was funded by the Deutsche Forschungsgemeinschaft (DFG) as part of the CRC 1123 (Z1) and of the Gottfried Wilhelm Leibniz Prize [2013; NT 3/10-1]. The authors thank the Italian Ministry of Education, University and Research* (PONa3_00395 "Bioscience & Health") for support.

Open access funding enabled and organized by Projekt DEAL.

Conflict of Interest

The authors declare no conflict of interest.

Data Availability Statement

Research data are not shared.

Keywords

fullerenes, lysozymes, multimodal microscopy, optoacoustic imaging, photodynamic therapy, phototheranostic agents

Received: February 12, 2021
Published online: March 9, 2021

[1] L. Cheng, C. Wang, Z. Liu, *Chem. Rev.* **2014**, *114*, 10869.
[2] H. Xiang, Y. Chen, *Small* **2019**, *15*, 1.
[3] J. Bhaumik, A. K. Mittal, A. Banerjee, Y. Chisti, U. C. Banerjee, *Nano Res.* **2015**, *8*, 1373.
[4] L. Guo, G. Niu, X. Zheng, J. Ge, W. Liu, Q. Jia, P. Zhang, H. Zhang, P. Wang, *Adv. Sci.* **2017**, *4*, 1700085.
[5] P. Agostinis, K. Berg, K. A. Cengel, T. H. Foster, A. W. Girotti, S. O. Gollnick, S. M. Hahn, M. R. Hamblin, A. Juzeniene, D. Kessel, M. Korbelik, J. Moan, P. Mroz, D. Nowis, J. Piette, B. C. Wilson, J. Golab, *Ca-Cancer J. Clin.* **2011**, *61*, 250.
[6] S. S. Lucky, K. C. Soo, Y. Zhang, *Chem. Rev.* **2015**, *115*, 1990.
[7] Y. Liu, P. Bhattarai, Z. Dai, X. Chen, *Chem. Soc. Rev.* **2019**, *48*, 2053.
[8] D. Gao, X. Guo, X. Zhang, S. Chen, Y. Wang, T. Chen, G. Huang, Y. Gao, Z. Tian, Z. Yang, *Mater. Today Bio.* **2020**, *5*, 100035.
[9] A. B. Ormond, H. S. Freeman, *Materials* **2013**, *6*, 817.
[10] A. Cantelli, G. Battistelli, G. Guidetti, J. Manzi, M. Di Giosia, M. Montalti, *Dyes Pigm.* **2016**, *135*, 64.
[11] J. H. Park, D. S. Dumani, A. Arsiwala, S. Emelianov, R. S. Kane, *Nanoscale* **2018**, *10*, 15365.
[12] C. Xu, F. Chen, H. F. Valdovinos, D. Jiang, S. Goel, B. Yu, H. Sun, T. E. Barnhart, J. J. Moon, W. Cai, *Biomaterials* **2018**, *165*, 56.
[13] J. U. Menon, P. Jadeja, P. Tambe, K. Vu, B. Yuan, K. T. Nguyen, *Theranostics* **2013**, *3*, 152.
[14] I. L. Medintz, H. T. Uyeda, E. R. Goldman, H. Mattoussi, *Nat. Mater.* **2005**, *4*, 435.
[15] A. C. S. Samia, X. Chen, C. Burda, *J. Am. Chem. Soc.* **2003**, *51*, 15736.
[16] S. Zhang, D. Yang, D. Jing, H. Liu, L. Liu, Y. Jia, M. Gao, L. Guo, Z. Huo, *Nano Res.* **2014**, *7*, 1659.
[17] M. Lan, S. Zhao, W. Liu, C. S. Lee, W. Zhang, P. Wang, *Adv. Healthcare Mater.* **2019**, *8*, 1900132.
[18] C. Yi, Z. Yu, Q. Ren, X. Liu, Y. Wang, X. Sun, S. Yin, J. Pan, X. Huang, *Photodiagn. Photodyn. Ther.* **2020**, *30*, 101694.
[19] K. D. Patel, R. K. Singh, H. W. Kim, *Mater. Horiz.* **2019**, *6*, 434.
[20] S. Goodarzi, T. Da Ros, J. Conde, F. Sefat, M. Mozafari, *Mater. Today* **2017**, *20*, 460.
[21] E. Nakamura, H. Isobe, *Acc. Chem. Res.* **2003**, *36*, 807.
[22] E. Castro, A. H. Garcia, G. Zavala, L. Echegoyen, *J. Mater. Chem. B* **2017**, *5*, 6523.
[23] A. Dellinger, Z. Zhou, J. Connor, A. Madhankumar, S. Pamujula, C. M. Sayes, C. L. Kepley, *Nanomedicine* **2013**, *8*, 1191.
[24] R. Partha, J. L. Conyers, *Int. J. Nanomed.* **2009**, *4*, 261.
[25] S. Bosi, T. Da Ros, G. Spalluto, M. Prato, *Eur. J. Med. Chem.* **2003**, *38*, 913.
[26] N. Martín, *Chem* **2019**, *5*, 733.
[27] P. Mroz, G. P. Tegos, H. Gali, T. Wharton, T. Sarna, M. R. Hamblin, *Photochem. Photobiol. Sci.* **2007**, *6*, 1139.
[28] Z. Markovic, V. Trajkovic, *Biomaterials* **2008**, *29*, 3561.
[29] M. R. Hamblin, *Photochem. Photobiol. Sci.* **2018**, *17*, 1515.
[30] S. K. Sharma, L. Y. Chiang, M. R. Hamblin, *Nanomedicine* **2011**, *6*, 1813.
[31] V. Krishna, N. Stevens, B. Koopman, B. Moudgil, *Nat. Nanotechnol.* **2010**, *5*, 330.
[32] V. Krishna, A. Singh, P. Sharma, N. Iwakuma, Q. Wang, Q. Zhang, J. Knapik, H. Jiang, S. R. Grobmyer, B. Koopman, B. Moudgil, *Small* **2010**, *6*, 2236.
[33] Y. Lyu, Y. Fang, Q. Miao, X. Zhen, D. Ding, K. Pu, *ACS Nano* **2016**, *10*, 4472.
[34] M. R. Hamblin, H. Abrahamse, *Antibiotics* **2020**, *9*, 53.
[35] N. Yumita, T. Watanabe, F.-S. Chen, Y. Momose, S.-I. Umemura, *Anticancer Res.* **2016**, *36*, 2665.
[36] N. Yumita, Y. Iwase, T. Imaizumi, A. Sakurazawa, Y. Kaya, K. Nishi, T. Ikeda, S. I. Umemura, F. S. Chen, Y. Momose, *Anticancer Res.* **2013**, *33*, 3145.
[37] Z. Chen, L. Ma, Y. Liu, C. Chen, *Theranostics* **2012**, *2*, 238.
[38] F. Z. Henari, S. MacNamara, O. Stevenson, J. Callaghan, D. Weldon, W. J. Blau, *Adv. Mater.* **1993**, *5*, 930.
[39] A. Mateo-Alonso, K. Iliopoulos, S. Couris, M. Prato, *J. Am. Chem. Soc.* **2008**, *130*, 1534.
[40] P. Aloukos, K. Iliopoulos, S. Couris, D. M. Guldi, C. Sooambar, A. Mateo-Alonso, P. G. Nagaswaran, D. Bonifazi, M. Prato, *J. Mater. Chem.* **2011**, *21*, 2524.
[41] S. R. Chae, A. R. Badireddy, J. F. Budarz, S. Lin, Y. Xiao, M. Therezien, M. R. Wiesner, *ACS Nano* **2010**, *4*, 5011.
[42] D. M. Guldi, M. Prato, *Acc. Chem. Res.* **2000**, *33*, 695.
[43] E. M. Hotze, J. Labille, P. Alvarez, M. R. Wiesner, *Environ. Sci. Technol.* **2008**, *42*, 4175.
[44] J. Lee, Y. Yamakoshi, J. B. Hughes, J.-H. Kim, *Environ. Sci. Technol.* **2008**, *42*, 3459.
[45] D. Antoku, K. Sugikawa, A. Ikeda, *Chem. – Eur. J.* **2019**, *25*, 1854.
[46] S. Anju, J. Ashtami, P. V. Mohanan, S. Anju, J. Ashtami, P. V. Mohanan, *Gen. Chem.* **2020**, *6*, 190022.
[47] J. Ashtami, S. Anju, P. V. Mohanan, *Colloids Surf., B* **2019**, *184*, 110530.
[48] M. Di Giosia, P. H. H. Bomans, A. Bottoni, A. Cantelli, G. Falini, P. Franchi, G. Guarracino, H. Friedrich, M. Lucarini, F. Paolucci, S. Rapino, N. A. J. M. Sommerdijk, A. Soldà, F. Valle, F. Zerbetto, M. Calvaresi, *Nanoscale* **2018**, *10*, 9908.
[49] M. Calvaresi, F. Arnesano, S. Bonacchi, A. Bottoni, V. Calò, S. Conte, G. Falini, S. Fermani, M. Losacco, M. Montalti, G. Natile, L. Prodi, F. Sparla, F. Zerbetto, *ACS Nano* **2014**, *8*, 1871.
[50] M. Di Giosia, F. Nicolini, L. Ferrazzano, A. Soldà, F. Valle, A. Cantelli, T. D. Marforio, A. Bottoni, F. Zerbetto, M. Montalti, S. Rapino, A. Tolomelli, M. Calvaresi, *Bioconjugate Chem.* **2019**, *30*, 808.
[51] M. Liutkus, A. López-Andarias, S. H. Mejías, J. López-Andarias, D. Gil-Carton, F. Feixas, S. Osuna, W. Matsuda, T. Sakurai, S. Seki, C. Atienza, N. Martín, A. L. Cortajarena, *Nanoscale* **2020**, *12*, 3614.
[52] K.-H. Kim, D.-K. Ko, Y.-T. Kim, N. H. Kim, J. Paul, S.-Q. Zhang, C. B. Murray, R. Acharya, W. F. DeGrado, Y. H. Kim, G. Grigoryan, *Nat. Commun.* **2016**, *7*, 11429.
[53] S. J. Vance, V. Desai, B. O. Smith, M. W. Kennedy, A. Cooper, *Biophys. Chem.* **2016**, *214–215*, 27.
[54] A. Soldà, A. Cantelli, M. Di Giosia, M. Montalti, F. Zerbetto, S. Rapino, M. Calvaresi, *J. Mater. Chem. B* **2017**, *5*, 6608.
[55] A. Ikeda, M. Matsumoto, M. Akiyama, J. I. Kikuchi, T. Ogawa, T. Takeya, *Chem. Commun.* **2009**, *12*, 1547.
[56] A. Ikeda, Y. Doi, M. Hashizume, J. I. Kikuchi, T. Konishi, *J. Am. Chem. Soc.* **2007**, *129*, 4140.
[57] Y. Doi, A. Ikeda, M. Akiyama, M. Nagano, T. Shigematsu, T. Ogawa, T. Takeya, T. Nagasaki, *Chem. – Eur. J.* **2008**, *14*, 8892.
[58] M. Calvaresi, A. Bottoni, F. Zerbetto, *J. Phys. Chem. C* **2015**, *119*, 28077.
[59] D. Callerio-Babudieri, *Nature* **1966**, *212*, 1274.
[60] T. Kooistra, A. M. Duursma, J. M. W. Bouma, M. Gruber, *Biochim. Biophys. Acta, Gen. Subj.* **1980**, *631*, 439.
[61] S. Lin, J. Reppert, Q. Hu, J. S. Hudson, M. L. Reid, T. A. Ratnikova, A. M. Rao, H. Luo, P. C. Ke, *Small* **2009**, *5*, 72.
[62] P. Sharma, N. Verma, P. K. Singh, S. Korpole, Ashish, *Sci. Rep.* **2016**, *6*, 22475.
[63] A. Gollmer, J. Arnbjerg, F. H. Blaikie, B. W. Pedersen, T. Breitenbach, K. Daasbjerg, M. Glasius, P. R. Ogilby, *Photochem. Photobiol.* **2011**, *87*, 671.
[64] Y. Yamakoshi, N. Umezawa, A. Ryu, K. Arakane, N. Miyata, Y. Goda, T. Masumizu, T. Nagano, *J. Am. Chem. Soc.* **2003**, *125*, 12803.
[65] R. W. Redmond, J. N. Gamlin, *Photochem. Photobiol.* **1999**, *70*, 391.
[66] T. Yogo, Y. Urano, A. Mizushima, H. Sunahara, T. Inoue, K. Hirose, M. Iino, K. Kikuchi, T. Nagano, *Proc. Natl. Acad. Sci. U. S. A.* **2008**, *105*, 28.
[67] T. Zang, Y. Xie, S. Su, F. Liu, Q. Chen, J. Jing, R. Zhang, G. Niu, X. Zhang, *Angew. Chem., Int. Ed.* **2020**, *59*, 10003.
[68] D. Soliman, G. J. Tserevelakis, M. Omar, V. Ntziachristos, *Sci. Rep.* **2015**, *5*, 12902.

[69] M. Seeger, A. Karlas, D. Soliman, J. Pelisek, V. Ntziachristos, *Photoacoustics* **2016**, *4*, 102.
[70] S. Kellnberger, D. Soliman, G. J. Tserevelakis, M. Seeger, H. Yang, A. Karlas, L. Prade, M. Omar, V. Ntziachristos, *Light: Sci. Appl.* **2018**, *7*, 109.
[71] C. Massner, F. Sigmund, S. Pettinger, M. Seeger, C. Hartmann, N. P. Ivleva, R. Niessner, H. Fuchs, M. H. de Angelis, A. Stelzl, N. L. Koonakampully, H. Rolbieski, U. Wiedwald, M. Spasova, W. Wurst, V. Ntziachristos, M. Winklhofer, G. G. Westmeyer, *Adv. Funct. Mater.* **2018**, *28*, 1706793.
[72] G. J. Tserevelakis, D. Soliman, M. Omar, V. Ntziachristos, *Opt. Lett.* **2014**, *39*, 1819.
[73] M. Seeger, D. Soliman, J. Aguirre, G. Diot, J. Wierzbowski, V. Ntziachristos, *Nat. Commun.* **2020**, *11*, 2910.
[74] A. Grebinyk, S. Grebinyk, S. Prylutska, U. Ritter, O. Matyshevska, T. Dandekar, M. Frohme, *Free Radical Biol. Med.* **2018**, *124*, 319.
[75] A. Dellinger, Z. Zhou, S. K. Norton, R. Lenk, D. Conrad, C. L. Kepley, *Nanomed.: Nanotechnol., Biol. Med.* **2010**, *6*, 575.
[76] N. Shirasu, S. O. Nam, M. Kuroki, *Anticancer Res.* **2013**, *33*, 2823.
[77] D. Antoku, S. Satake, T. Mae, K. Sugikawa, H. Funabashi, A. Kuroda, A. Ikeda, *Chem. – Eur. J.* **2018**, *24*, 7335.
[78] Z. Du, N. Gao, X. Wang, J. Ren, X. Qu, *Small* **2018**, *14*, 1801852.
[79] H. Shi, R. Gu, W. Xu, H. Huang, L. Xue, W. Wang, Y.-W. Zhang, W. Si, X. Dong, *ACS Appl. Mater. Interfaces* **2019**, *11*, 44970.